Journal of Coastal Research	37	6	1181–1192	Coconut Creek, Florida	November 2021

Seasonal and Daily Variation of Hydrodynamic Conditions in the Amazon River Mouth: Influence of Discharge and Tide on Flow Velocity

Diani F.S. Less[†‡]*, Nicholas D. Ward[§††], Jeffrey E. Richey[††], and Alan C. Da Cunha[‡‡]

[†]Institute of Water Science and Technology
Federal University of Western Pará (UFOPA)
Santarém, PA, Brazil

[‡]Post-Graduate Program Bionorte
Federal University of Amapá (UNIFAP)
Macapá, AP, Brazil

[§]Marine and Coastal Research Laboratory
Pacific Northwest National Laboratory
Sequim, WA 98382, U.S.A.

[††]School of Oceanography
University of Washington
Seattle, WA 98195, U.S.A.

[‡‡]Department of Civil Engineering
UNIFAP
Macapá, AP, Brazil

www.cerf-jcr.org

www.JCRonline.org

ABSTRACT

Less, D.F.S.; Ward, N.D.; Richey, J.E., and Da Cunha, A.C., 2021. Seasonal and daily variation of hydrodynamic conditions in the Amazon River Mouth: Influence of discharge and tide on flow velocity. *Journal of Coastal Research,* 37(6), 1181–1192. Coconut Creek (Florida), ISSN 0749-0208.

Hydrodynamics characteristics control various biogeochemical processes related to the phenomena of transport of particulate materials, biogeochemical components, and greenhouse emissions; however, the hydrodynamic conditions in the North Channel of the Amazon River Mouth is relatively little understood. The seasonal and tidal variability of hydrodynamic characteristics in the North Channel of the Amazon River Mouth were investigated using an acoustic measurement technique. The measurements of discharge (Q), water velocity (U), and water level (h) were performed during a semidiurnal tidal cycle in a 12 km wide transect during four hydrological seasons. The hydrodynamics are mainly controlled by the river discharge, being directly related to the rain pattern with a well-defined time lapse for the Amazon Basin. The amplitude of the tides, the mean discharge, and the velocity of the natural flow presented during high discharge season were 3 m, 12,423 $m^3\ s^{-1}$ and 1.18 $m\ s^{-1}$, respectively. The analyses of tidal effects showed a phase opposition between the water level, river discharge, and water velocity; the water velocity was ~42% higher during the ebb tide with a duration ~1 hour and 30 minutes longer than the flood phase. The U and h are inversely proportional ($R = -0.72$, $p < 0.01$); significant variations in velocity throughout the tidal cycle are associated with the highest values observed at ebb tide, when the velocity and level of the water are significantly influenced by both diurnal and seasonal components. Thus, the results can contribute to the evaluations of more detailed potential interactions of the advective processes, such as mixing and dilution of passive agents of the natural flow, which are very poorly recorded in the existing literature.

ADDITIONAL INDEX WORDS: *Hydrodynamics, river-tide interactions, estuaries, Acoustic Doppler Current Profiler.*

INTRODUCTION

Estuaries are transitional areas between oceans and inland waters where hydrodynamic processes are controlled by oceanic tidal waves and fluvial discharges (McLusky and Elliott, 2004; Zhang *et al.,* 2018). In addition, these hydrodynamic processes control the flow of sediments, nutrients, biogeochemical components, and the emission of gases, which are transferred from soil and rivers to the atmosphere, coastal area (*e.g.*, mangroves, estuaries, deltas) and the ocean (Ward *et al.,* 2017, 2020). These processes are mainly influenced by the weather, especially rainfall, which results in significant variability in river discharge (Freitas *et al.,* 2017; Santos *et al.,* 2018).

Interactions between land, river, and ocean and the variability of water hydrodynamic conditions play an important role in the transfer, exchange, and dispersion of sediments transported by rivers. These interactions impact estuarine deposits, coastal deposits, erosion, and accumulation areas (Ji, Pan, and Chen, 2020). In this way, the upstream water flows are significant modulators of the environmental characteristics of estuaries due to the contribution and transport of particulate and dissolved compounds (Garel and D'alimonte, 2017; Haslet, 2009; Montagna, Palmer, and Pollack, 2013).

In coastal ecosystems, ideal hydrodynamic conditions and the large supply of allochthonous and autochthonous organic matter transported by rivers enable the intense processing of these compounds, modifying their structure and concentration. Many studies describe estuaries as heterotrophic systems that filter terrestrial materials, with the majority classified as a source of carbon dioxide (CO_2) to the atmosphere. For these reasons, estuaries are characterized as important components of the global and regional carbon cycle (Abril *et al.,* 2000; Borges and Abril, 2011; Cai *et al.,* 1999; Frankignoulle *et al.,* 1998; Valerio *et al.*, 2021).

Under natural conditions, tidal rivers usually exhibit temporal variability of their hydrodynamic conditions, including tidal fluctuations and seasonal variations of discharge (Kosuth *et al.,* 2009; Matte, Secretan, and Morin, 2014). The seasonal variability of discharge is a key component of hydrodynamic patterns in river systems, and daily variability

DOI: 10.2112/JCOASTRES-D-21-00010.1 received 21 January 2021; accepted in revision 24 June 2021; corrected proofs received 29 July 2021; published pre-print online 30 August 2021.
*Corresponding author: diani.less@ufopa.edu.br

is equally important in tidal systems (Abreu *et al.,* 2020; Cunha *et al*., 2021). During the past two decades, the scientific community has recognized the importance of the lower reaches of rivers and the coastal zone to the global carbon cycle (Borges, 2005; Cai, 2011; Sawakuchi *et al.,* 2017; Wollast, 1998). However, the role of estuaries and their influence on hydrodynamic conditions remains uncertain. This uncertainty can be attributed to geographic size and complexity; geomorphology; high spatial and temporal heterogeneity; variable hydrological conditions; and the tide, wave, and wind features of estuaries dominated by the river or ocean (Borges, 2005; Chen *et al.,* 2013).

Another important aspect is the insufficient quantity of information related to tropical estuaries, especially the lower reaches of major tropical rivers such as the Amazon and Congo Rivers, compared with that of temperate and boreal estuaries (Cotovicz *et al.,* 2016; Richey *et al.,* 2021). There are few studies related to hydrodynamic conditions in the lower Amazon River (Gabioux, Vinzon, and Paiva, 2005; Kosuth *et al.,* 2009; Rosário, Bezerra, and Vinzón, 2009). Considering the global importance of the Amazon River, investigations related to the drivers and influencing factors of its hydrodynamic behavior are necessary to understand biogeochemical cycles and climate change scenarios (Abreu *et al.,* 2020). In addition, that information is essential to allow future calibration of numerical models (Abreu *et al.,* 2020; Cunha *et al.,* 2021).

The Amazon River is the largest river system in the world; it discharges ~16%–20% of the world's fresh water to the ocean, emitting 25% of CO_2 from inland waters to the atmosphere and transporting approximately 1.2×10^9 tons of suspended sediments per year. Thus, its plume extends up to 1.39×10^6 km^2 into the Atlantic Ocean (Chong *et al.,* 2016; Raymond *et al.,* 2013; Richey *et al.,* 2002; Valerio *et al.,* 2021).

Tidal effects can be observed along the lower Amazon River up to 1000 km from the mouth of the river, with a more significant influence observed at the Almeirim station located 500 km upstream of the mouth (Kosuth *et al.,* 2009; Ward *et al.,* 2015). This occurs because the oceanic tidal waves propagate along estuaries and up the lower reaches of rivers when gradients are low. Thus, the Amazon River presents a very low gradient along its lower 1200 km, with 11.5 mm km^{-1} between Ponta do Céu and Santarém (Kosuth *et al.,* 2009).

At the mouth, the river flow reverses and is completely influenced by the semidiurnal tidal cycle, increasing the residence time of the water and the vertical mixing. This promotes the daily connectivity between coastal water bodies (primarily lakes) and enhances the exchange of energy and materials between the soil, river, atmosphere, and Atlantic Ocean (Cunha and Sternberg, 2018; Freitas *et al.,* 2017; Kosuth *et al.,* 2009).

Considering this scenario, the present study aims to fill a relevant scientific gap about the seasonal variability of hydrodynamics in a representative stretch of the lower Amazon River, the North Channel of the Amazon River Mouth, by describing for the first time the seasonal patterns of tide–river dynamics and the possible influence of an intense seasonal cycle of rainfall. An Acoustic Doppler Current Profiler (ADCP) was used in this investigation to capture rapid discharge measurements, and it continuously monitored the variations in discharge during the tidal cycle (Guyot, Filizola, and Guimarães, 1998; Kosuth *et al.,* 2009).

These data can support ecological studies such as the quantification of nutrient flux, greenhouse emissions, sedimentation processes, oxygen balance, mineralization, and primary production. Sanitation issues such as self-depuration, residence time, and dilution capacity may be addressed as well (Abreu *et al.,* 2020; Braunschweig *et al.,* 2003; Cunha *et al*., 2021; Gagne-Maynard *et al.,* 2017; Sawakuchi *et al.,* 2017; Valerio *et al.,* 2018; Ward *et al.,* 2016).

This study investigated the hypothesis that the hydrodynamic behavior of the lower reaches of the Amazon River, particularly water velocity, is strongly influenced by seasonal and daily variation of river discharge and tidal amplitude. It is hypothesized that the highest water velocities would be observed during the ebb tide in the deepest zones of the channel due to, in part, the decreased influence of bed friction. In this way, it is expected that velocity has an inversely proportional relationship with river depth.

METHODS

The influence of seasonal and diurnal tidal cycles on the hydrodynamic conditions (discharge, water velocity, and water level) of the North Channel, mouth of the Amazon River, was analyzed based on measurements performed during the four hydrological seasons (rising, high, falling, and low water) between 2014 and 2016.

Study Area

Four field campaigns were conducted between 2014 and 2016 in a section of the North Channel (00°04′841″ S, 50°59′624″ W) of the Amazon River Mouth (Figure 1). Approximately 30% of the discharge of the Amazon River flows through the North Channel (Ward *et al.,* 2017). This stretch is influenced by mesotides that drive a variation of about ~2.8 m in the water column amplitude with a reversal of river flow. This flow reversal does not result in any changes in salinity or seawater influence due to the high freshwater discharge (Sawakuchi *et al.,* 2017). At a location 150 km downstream of Macapá, the channel width continues to increase and is distributed between large islands until it disconnects from the mainland and the riparian zone (Cai, 2011; Cunha and Sternberg, 2018; Ward *et al.,* 2015). The water mass that flows into the ocean still retains its freshwater characteristics on the surface approximately 60 km from the mouth (Molinas *et al.,* 2014; Valerio *et al.,* 2018).

Near the mouth of the Amazon River, the water flow reverses (flood and ebb). This increases the connectivity of the main channel with large, flooded areas, lakes, and adjacent channels (Cunha and Stenberg, 2018; Santos *et al.,* 2018) in addition to significant tributaries (Eom, Seo, and Ryu, 2017; Sawakuchi *et al.,* 2017). When mixed, the waters show the intense interaction capacity between runoff and water quality (Santos *et al.,* 2018).

Locally, the primary characteristics of the astronomical tide can usually be synthesized according to its periodic, predictable, and regular water-level oscillation. This magnitude is variable in level over periods of 12 hours (semidiurnal). Frequent tidal fluctuations caused by the flood and ebb phases are associated with tidal currents, with variable lagging

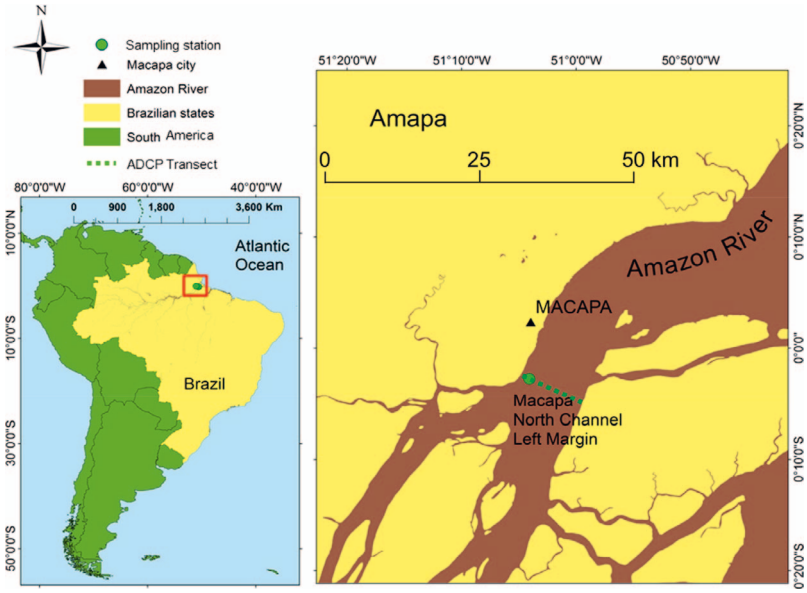

Figure 1. Study area and location of transects in the North Channel near the mouth of the Amazon River and the city of Macapá.

upstream and downstream depending on local conditions (Alfredini and Arasaki, 2009).

The mean water level at the river mouth gauging station Punta do Céu (0°45′54.37″ N, 50°7′7.33″ W) does not vary throughout the year (~0.04 m). This reflects the lack of influence of the Amazon River hydrological regime on the mean water level at Punta do Céu, which is related to the local mean sea level (Kosuth *et al.,* 2009). The semidiurnal tidal amplitude (difference between high tide and low tide water levels for a given tidal cycle) varies from 1.9 m to 4.5 m, with an average amplitude of 3.3 m. High amplitudes occur during the new moon or full moon phases (spring tidal or syzygy tidal), with maximum values in September–October and March–April (Abreu *et al.,* 2020; Kosuth *et al.,* 2009).

The climate of the study area is classified as tropical monsoon (category Am), according to the Köppen classification (Köppen, 2020); it is a tropical rainy monsoon climate, with a short period of rainfall of less than 60 mm per month (usually from September to November). The average monthly air temperature is 26.0 ± 0.4°C, with maximum and minimum values between 31.5 ± 0.7°C and 22.0 ± 0.3°C, respectively (Costa *et al.,* 2013).

The annual average rainfall and wind speed in the study area according to the last Climatological Normal (1981–2010) is 2450 mm and 3 m s^{-1}, respectively (National Institute of Meteorology – INMET, 2020).

For the Lower Amazon River, the hydrological seasons are classified as rising water (from January to March), high water (from April to June), falling water (from July to September), and low water (from October to December) (Valerio *et al.,* 2018). The experimental campaigns occurred on 20 September 2014 (falling water), 25 February 2015 (rising water), 6 October 2015 (low water), and 26 May 2016 (high water) during complete semidiurnal tidal cycles. These campaigns covered ebb (continental to ocean current), flood (reverse flow, ocean to mainland), and transitional times (between both extremes).

Hydrodynamic Measurements

The discharge (Q), depth (z), and water velocity (U) were measured with an ADCP, (Sontek Riversurveyor M9) during four field campaigns conducted between 2014 and 2016 according to the hydrological cycle. All measurements were performed during neap tides due to field logistics and to remove spring/neap variability as a confounding factor. For the lower sector of the Amazon River, where the river width can reach 12 km, the ADCP technique provided a precise measure of the river discharge in roughly 1 hour and monitored discharge variations in a tidal cycle.

Cross-channel transects with a width of 12 km were performed (approximately seven to eight times) using an ADCP during a semidiurnal tidal cycle (8 to 13 hours). This procedure is required to evaluate and quantify the flow reversal and net discharge (difference between ebb and flood tide), enabling the average river discharge and water velocity from the section to be precisely calculated (Cunha *et al.,* 2012; Sawakuchi *et al.,* 2017; Ward *et al.,* 2016).

Velocity, depth, and discharge data were collected using aboard the B/M Mirage vessel equipped with an ADCP. Velocity profiles were obtained as ensembles averaged over 5 seconds in cells 0.5 m thick.

Water level (h) was obtained from the National Oceanographic Data Bank belonging to the Brazilian Navy relative to the Porto de Santana station (0°3′25.17″ N; 51°10′50.7″ W) located at the North Channel near the city of Macapá.

For the accompanying seasonal data of local rainfall (Macapá) and rainfall at the beginning of the Lower Amazon River (Óbidos) located 900 km from the sampling station, monthly rainfall data (2014–16) were obtained from the

Table 1. *Net discharge (Q), water velocity (U), depth, and water level (mean ± standard deviation) measured during four hydrological regimes in the Northern Channel of the lower Amazon River between 2014 and 2016.*

Date	Season	Discharge $10^{-3} \times (m^3\ s^{-1})$	Water Velocity (m s^{-1})	Depth (m)	Water Level (m)
25 February 2015	Rising	124.23 ± 129.62	0.43 ± 0.89	16.34 ± 0.62	1.74 ± 0.91
26 May 2016	High	100.61 ± 143.06	0.53 ± 0.68	18.29 ± 0.92	1.79 ± 1.00
20 September 2014	Falling	63.42 ± 123.41	0.29 ± 0.63	17.86 ± 0.74	1.75 ± 0.87
6 October 2015	Low	55.18 ± 111.45	0.26 ± 0.57	18.14 ± 0.65	1.71 ± 0.78

National Institute of Meteorology (National Institute of Meteorology – INMET, 2021) from the Óbidos historic downstream gauging station (82178, 01°54′05″ S, 55°31′07″ W) and Macapá (82098, 00°03′00″ N, -51°04′00) meteorological stations.

Statistical Analyses

All variables were analyzed using descriptive statistics, by which the means and standard deviations were generated. In addition, statistical analysis of hypotheses such as the Shapiro-Wilk test ($p < 0.05$) was applied to test the normality of the distribution of the variables. For hypothesis testing of the significant differences among the hydrological seasons and tidal phases, ebb and flood were applied to the Kruskal-Wallis and Mann-Whitney nonparametric tests, respectively. Spearman correlation and linear regression models were used to correlate the dependent (U) and independent variables (Q and h). A confidence level of 95% ($p < 0.05$) was applied in the statistical analyses, which were all performed with the R software (R Project for Statistical Computing, 2021).

RESULTS

Discharge, water velocity, water level, depth, and rainfall data collected in the field campaigns performed between 2014 and 2016 and database analyses were organized considering seasonal and daily variation (tidal cycles).

Seasonal Variation of Hydrodynamic Parameters

The highest net discharge obtained between 2014 and 2016 was during the rising-water season (124,233 ± 129,622 $m^3\ s^{-1}$), followed by the high-water season (100,608 ± 143,058 $m^3\ s^{-1}$). The average discharges during the falling- and low-water seasons were 63,423 ± 123,413 $m^3\ s^{-1}$ and 55,183 ± 111,449 $m^3\ s^{-1}$, respectively (Table 1, Figure 2a). No significant variation in discharge occurred between hydrological periods (Kruskal-Wallis, $p > 0.05$), likely due to the high variability imposed by the tidal flow reversal. However, considering the tidal phases, discharge reached 233,119 $m^3\ s^{-1}$ during the ebb phase, indicating a significant diurnal variation (Mann-Whitney, $p < 0.01$), Figure 2b).

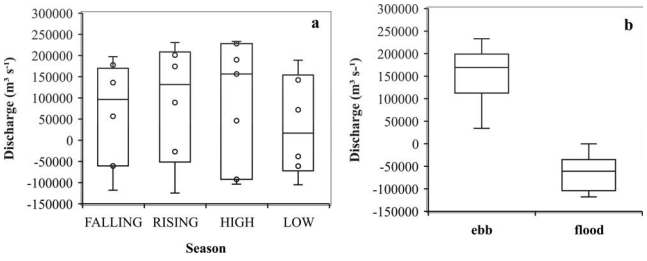

Figure 2. (a) Seasonal variability of river discharge and (b) diurnal variability of discharge in the North Channel of the Amazon River Mouth between 2014 and 2016.

The highest values of velocity were obtained during the high- and rising-water seasons (0.53 ± 0.68 m s^{-1} and 0.43 ± 0.89 m s^{-1}, respectively). The lowest value (0.26 ± 0.57 m s^{-1}) was observed during the low-water season; during the falling water season, the mean was 0.29 ± 0.63 m s^{-1} (Table 1, Figure 3a). No significant variation in the water velocity occurred between hydrological periods, but significant diurnal variation occurred in the tidal phases (Kruskal-Wallis, $p < 0.01$), where the mean water velocity in the ebb phase was 0.78 ± 0.28 m s^{-1} and was –0.47 ± 0.17 m s^{-1} in the flood phase (Mann-Whitney, $p < 0.01$, Figure 3b).

In the low-water season, the average water velocity was –0.38 ± 0.06 m s^{-1} at flood tide and 0.64 ± 0.28 m s^{-1} at ebb tide (Figure 4a,b). During the rising-water season, the average velocity was –0.69 ± 0.29 m s^{-1} at flood phase and 0.99 ± 0.20 m s^{-1} at ebb phase (Figure 4c,d). The variation and flow reversals were captured through the profile depicted in Figure 4a; water velocity can substantially decrease regardless of depth (*e.g.*, the left margin in Figure 4a). At other time intervals, water velocity tended to be higher at the deepest part of the channel. During the low-water season, water velocity was higher near the right margin during flood tide, whereas at ebb tide, U was higher near the left margin. During rising-water season at flood tide, the water velocity was higher near the left margin, whereas during ebb tide, U was similar near both margins.

It is important to note that tidal amplitude fluctuations occur that add to seasonal hydrological variations. The highest depth value was obtained during the high-water season (18.29 ± 0.92 m). The lowest mean value was obtained during the rising-water season (16.34 ± 0.62 m). During the falling- and low-water seasons, the depths were 17.86 ± 0.74 m and 18.14 ± 0.65 m, respectively (Table 1, Figure 5). The depth showed significant differences between hydrological periods (Kruskal-Wallis, $p < 0.05$). The longitudinal variations of depth show the presence of three subchannels: Depth in the first subchannel (from the left to the right side of the channel) reached ≈28 m, the central part of the channel had ≈18 m, and the right side reached 27 m.

The highest mean water level was obtained during the high-water season (1.79 ± 1.00 m). The lowest value was observed during the low-water season (1.71 ± 0.78 m). During the falling- and rising-water seasons, the mean water levels were 1.75 ± 0.87 m and 1.74 ± 0.91, respectively (Table 1, Figure 6a). Tidal amplitude (Figure 6b) was higher during the high-water season (2.97 m), and the lowest value (2.32 m) was obtained during the low-water season. However, no significant variation occurred in the mean water level between the

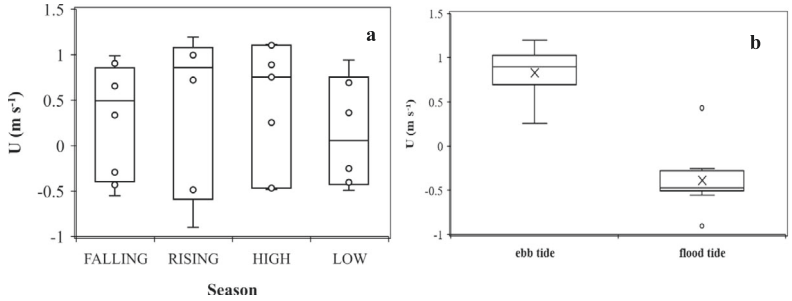

Figure 3. (a) Seasonal variation in the water velocity and (b) tidal phase (ebb and flood) variation in the water velocity in the North Channel of the Amazon River Mouth between 2014 and 2016.

hydrological periods (Kruskal-Wallis, $p > 0.05$). It is important to note that this nonsignificant variation corroborates the hypothesis of the depth averages in Figure 4a–d; however, this is due to the relatively high depth scale of the Lower Amazon River along this reach.

The highest rainfall obtained between 2014 and 2016 at Óbidos was during the high-water season (404 mm, April 2014, Figures 7 and 8a) followed by rising-water season (381 mm, March 2016, Figures 7 and 8a). Following this pattern, rainfall at Macapá was 584 and 554 mm during the same high- and

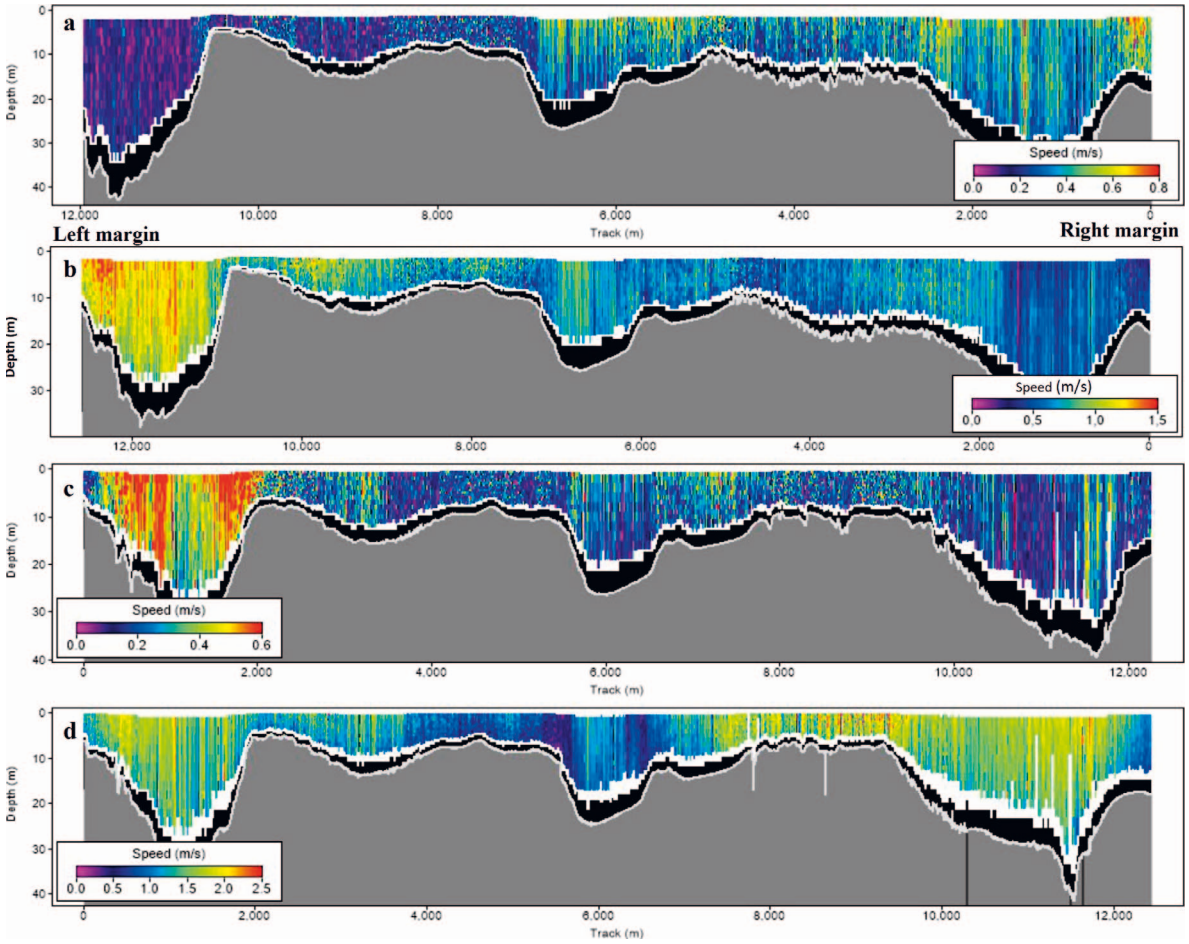

Figure 4. Water velocity in the low water ([a] flood and [b] ebb tide) and rising water seasons ([c] flood and [d] ebb tide) in the North Channel of the Amazon River Mouth, from the left to the right margin of the channel.

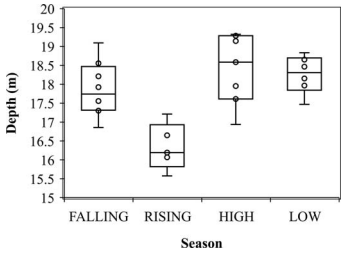

Figure 5. Seasonal variability of the depth in the North Channel of the Amazon River Mouth between 2014 and 2016.

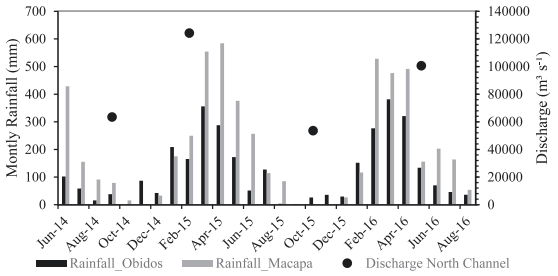

Figure 7. Monthly precipitation in Óbidos and Macapá between 2014 and 2016 and the net discharge measured in the four hydrological periods in the North Channel of the Amazon River Mouth.

rising-water seasons, respectively (Figures 7 and 8b). The annual variability was more relevant at Óbidos (Figure 8, Table 2), where the accumulated rainfall was higher in 2014 (1812 mm) compared with 2016 (1530 mm) and 2015 (1465 mm). At Macapá, accumulated rainfall was 2529 mm in 2014, 2490 mm in 2016, and 2422 mm in 2015.

The average rainfall during high water season was 358 ± 144 mm at Macapá; at Óbidos the highest average was during rising water (261 ± 84 mm). The averages during falling- and low-water seasons were 39 ± 38 mm and 38 ± 24 mm at Óbidos and 85 ± 54 mm and 44 ± 94 mm at Macapá, respectively (Table 2, Figure 8a,b). Significant variation occurred in rainfall between hydrological periods (Kruskal-Wallis, $p < 0.01$). That is, the distance factor between Macapá and Óbidos, with approximately 900 km, is capable of causing significant differences in the pattern of rainfall (mm) in the same region.

Hydrodynamic Variability during the Tidal Cycle

During the field campaign of September 2014 (falling water), the discharge peak during ebb tide was 197,324 $m^3\ s^{-1}$. In the flood phase, the highest value was –117,884 $m^3\ s^{-1}$ (Figure 9a), with significant variability during the tidal phases (Kruskal-Wallis, $p < 0.05$). The water velocity U reached 0.99 m s^{-1} at ebb tide (197,324 $m^3\ s^{-1}$) and presented a strong and positive relationship with Q ($R^2 = 0.99$, $p < 0.05$, Figure 9b). The water level was high in the flood phase at 2.8 m, and during the ebb phase, the minimum value was 0.63 m (Figure 9c). This hydrodynamic (or hydraulic) pattern is quite regular and can be extremely useful, for example, for the elaboration of key curves. That is, elaborate curves that relate to $U = aQ^b$ and $z = cQ^d$ and then the installation of a representative hydrometeorological station for the stretch of the Lower Amazon River.

In the field campaign of February 2015 (rising water), the discharge peak during ebb tide was 230,754 $m^3\ s^{-1}$. During the flood phase, the highest value was –124,503 $m^3\ s^{-1}$ (Figure 10a). The net discharge presented significant variability during the tidal phases (Kruskal-Wallis, $p < 0.05$). The maximum water velocity reached 1.19 m s^{-1} at ebb tide (174,334 $m^3\ s^{-1}$) (Figure 10a) and presented a significant relationship with Q ($R^2 = 0.70$, $p < 0.05$, Figure 10b). The water level was high in the flood phase at 2.99 m, but during ebb phase, the lowest value was 0.57 m (Figure 10c).

In October 2015 (low water), the discharge peak during ebb tide was 189,052 $m^3\ s^{-1}$, and at the flood phase, the highest value was –104,954 $m^3\ s^{-1}$. The net discharge presented significant variability during the tidal phases (Kruskal-Wallis, $p < 0.05$). The maximum water velocity reached 0.94 m s^{-1} at ebb tide (189,052 $m^3\ s^{-1}$) (Figure 11a) and presented a significant and positive relationship with discharge ($R^2 = 0.98$, $p < 0.05$, Figure 11b). Similar to the other seasons, the water level was high in the flood phase at 2.85 m, and during ebb phase, the minimum value was 0.65 m (Figure 11c).

In May 2016 (high water), the discharge peak during ebb tide was 233.119 $m^3\ s^{-1}$. At the flood tide, the highest value was –103.636 $m^3\ s^{-1}$. The net discharge presented significant variability during the tidal phases (Kruskal-Wallis, $p < 0.05$). The maximum water velocity reached 1.11 m s^{-1} at ebb tide (232,339 $m^3\ s^{-1}$) (Figure 12a) and presented a strong positively

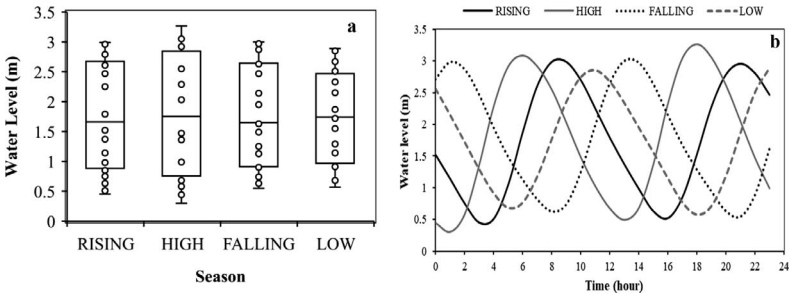

Figure 6. (a) Seasonal variability of the water level in the North Channel of the Amazon River Mouth between 2014 and 2016 (Porto de Santana station, 0°3′25.17″ N; 51° 10′50.7″ W). (b) Water level behavior during the tidal cycle during the four hydrological periods.

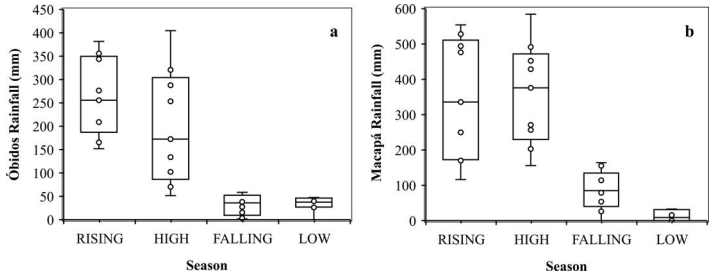

Figure 8. Seasonal variation in the rainfall at Óbidos (a) and Macapá (b) between 2014 and 2016.

relationship with discharge ($R^2 = 0.99$, $p < 0.05$) (Figure 12b). Following the pattern, water level was higher at the flood phase at 3.16 m, which was the highest value observed during all hydrological periods; however, during ebb phase, the minimum value was 0.58 m (Figure 12c).

DISCUSSION

The highest water flow was obtained in the rising water season (Table 1) in a measurement performed at the end of February 2015, and the second highest discharge was measured during the high-water season in May 2016. Considering that the Amazon River presents great regularity in the annual rainfall regime (Figure 7), there are well-defined variations in the flow rate and consequently in the velocity and depth of the rivers during the four hydrological periods (Callède *et al.,* 2002). The seasonal variability of the location of the Intertropical Convergence Zone promotes an intense seasonal cycle of rainfall in the Amazon Basin, specifically in the region of the Amazon River main channel (Fisch, Marengo, and Nobre, 1998; Marengo, 2009; Marengo and Espinoza, 2015; Marengo *et al.,* 2011; Wang and Fu, 2007).

Sea-surface temperature anomalies in the Pacific and Atlantic oceans influence variations in volume and the distribution of rainfall and discharge in the Amazon River Basin (Garel and D'alimonte, 2017; Marengo, 2009; Marengo *et al.,* 2011; Schöngart and Junk, 2007; Vale *et al.,* 2016). Years with decreased or increased rainfall due to the influence of El Niño or La Niña can consequently result in decreased or increased discharge in the river basin (Cunha and Sternberg, 2018; Vale *et al.,* 2016).

As a consequence, the occurrence of a strong El Niño event in 2015–16 (Jiménez-Muñoz *et al.,* 2016; Figure 7, Table 2) can explain the decreased discharge observed in the high-water season compared with that in the rising-water season, as well as the lack of significant seasonal variability. El Niño and La Niña events are becoming more frequent, resulting in increasingly common droughts and floods and causing changes in the hydrological cycle that impact river flow and associated physical and biogeochemical processes (Cunha and Sternberg, 2018; Gloor *et al.,* 2013; Vale *et al.,* 2016).

In relation to the seasonal variations of discharge, it is important to consider the existence of a time lag between the period of highest rainfall and the increase in discharge in the Amazon River. For the sectors located in the northern portion of the basin near the mainstem, the months of highest rainfall are March and April (Figure 7), and the months of maximum discharge are June and July. Likewise, other variables were related, such as water velocity (Figure 13) and water level. This effect is determined by the water residence time in the soil and the dynamics of the flooded areas (floodplains and igapós) and canals (Abreu *et al.,* 2020). Therefore, seasonal variations during the complete hydrological cycle (rising, high, falling, and low) between rivers in different regions of the Amazon basin occur at different periods, with a ~3 month time lapse in the flow of rivers that drain the southern (March–April) and northern portion (peaks between June and July) of the basin (Liebmann and Marengo, 2001).

The time lapse effects of the rain can also be observed when comparing discharge measured in the North Channel by Ward *et al*. (2018) in March 2016 (53,265 $m^3\ s^{-1}$) and discharge measured in the present study in May 2016 (100,608 $m^3\ s^{-1}$). This difference was likely influenced by the rainfall in February, March, and April 2016 (Figure 7).

The average discharge at rising water was similar to observed and predicted values obtained by Abreu *et al*. (2020). The discharge during the low-water season was similar to a measurement performed in November 2014 (61,539 $m^3\ s^{-1}$) by Ward *et al*. (2018).

As expected, the water velocity and water level increased in the hydrological periods with higher discharge (Table 1, Figure 4c,d, Figure 6) and were also influenced by the rainfall pattern (Figure 13). But, the tidal cycle U and the water level are inversely proportional, presenting a negative relationship (Spearman $R = –0.72$, $p < 0.01$, Table 3). As also expected, the results showed a phase opposition between the water level and river discharge (Spearman $R = –0.80$, $p < 0.01$, Table 3),

Table 2. *Seasonal and accumulated rainfall (year) at Macapá and Óbidos between 2014 and 2016.*

	Seasonal Rainfall (mm)				Accumulated Rainfall (mm)		
Station	Rising	High	Falling	Low	2014	2015	2016
Macapá	344 ± 172	358 ± 144	85 ± 54	44 ± 94	2529	2490	2422
Óbidos	261 ± 84	200 ± 123	39 ± 38	38 ± 24	1812	1465	1530

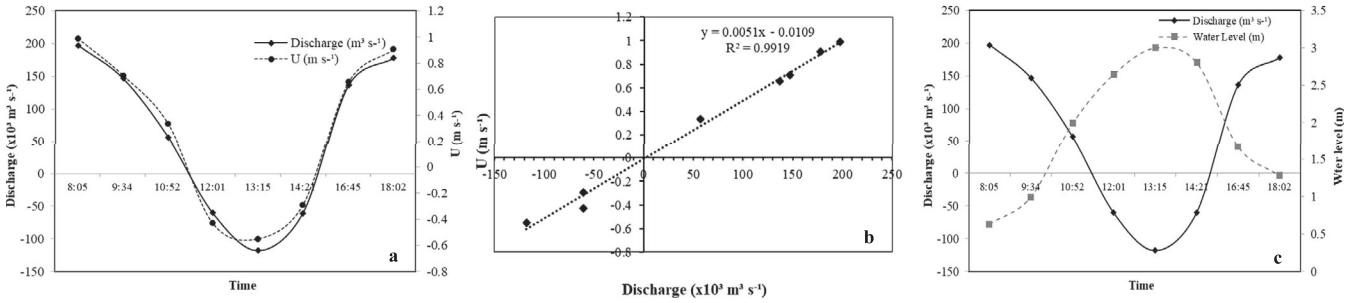

Figure 9. (a) Discharge and water velocity measured during the tidal cycle in the field campaign of September of 2014 (falling water) in the North Channel of the Amazon River Mouth. (b) Relationship between U and Q ($R^2 = 0.59$, $p < 0.05$). (c) Discharge and water level measured during the tidal cycle.

which is similar to results observed in other sections of the lower Amazon River (Kosuth *et al.,* 2009).

The tidal amplitude reached ~3 m during the high-water season, and the maximum difference in amplitude reached 0.65 m between the seasons. Compared with the spring tides that occurred in the period, there was an increase of 10 cm to 2 cm in water level, mainly at low-water season.

This result is similar to the experimental and predicted results found by Abreu *et al*. (2020) and Abril *et al*. (2013). This water-level oscillation indicates the storage and release of water, which causes the river discharge to decrease and increase, respectively. These results resemble a sine function with a decreased duration for the flood tide and an increased duration for the ebb tide, which can be related to the river flow resistance that slows down during falling tides and releases stored water after the flood tides. Thus, the water level does not decrease as rapidly as the sea level, which, when added to the duration of the tidal phases and their amplitude, demonstrates the intense and predominant influence of river discharge on specific hydrodynamic conditions, despite its relative proximity (~150 km) to the ocean (Kosuth *et al.,* 2009).

The amplifying function of river discharge can increase tidal amplitudes, especially during the high-water season, as observed in this and other studies (Table 1; Zhang *et al.,* 2018). Large tidal amplitudes can also be related to near-bottom fluid mud layers, which have an important impact on the tidal flow by reducing the energy loss and influencing the water level (Gabioux, Vinzon, and Paiva, 2005).

Tidal rivers are characterized by oscillatory and nonstationary gradients of water velocity and level and are controlled by interactions between river flow and tides (Abreu *et al.,* 2020; Cunha *et al*., 2021; Sassi and Hoitink, 2013). The storage and release of water controls the variability in river discharge, water level, and water velocity. The minimum or maximum discharge occurs at the maximum or minimum tidal level, respectively (Figures 9–12); this variation is also corroborated by Kosuth *et al*. (2009). This explains the higher water velocity observed during ebb tide (~42%, Figure 3b, Figure 4b–d), considering that the Q and U are directly proportional, which is similar to findings from other studies (Abreu *et al.,* 2020; Quesada *et al.,* 2019; Wang, Sun, and Zhao, 2020).

These relationships between tide and water velocity (Spearman $R = -0.72$, $p < 0.01$) were observed for all of the field campaigns (Figures 9–12). Velocity and net discharge were also directly proportional in all hydrological measurements and throughout the tidal cycle (Spearman $R = 0.91$, $p < 0.01$, Table 3). The flow reversal period was shorter (~4 h, 45 min) compared with the ebb period (~6 h, 15 min) and was similar to that measured by Abreu *et al*. (2020), Cunha *et al*. (2021), and Kosuth *et al*. (2009). As the water flow normalizes, the water velocity increases (Figure 4).

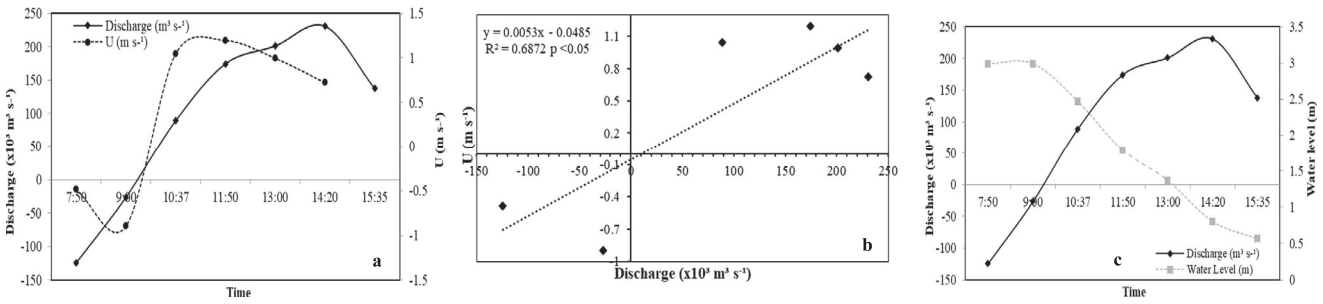

Figure 10. (a) Discharge and water velocity measured during the tidal cycle in the field campaign of February 2015 (rising water) in the North Channel of the Amazon River Mouth. (b) Relationship between U and Q ($R^2 = 0.30$, $p > 0.05$). (c) Discharge and water level measured during the tidal cycle.

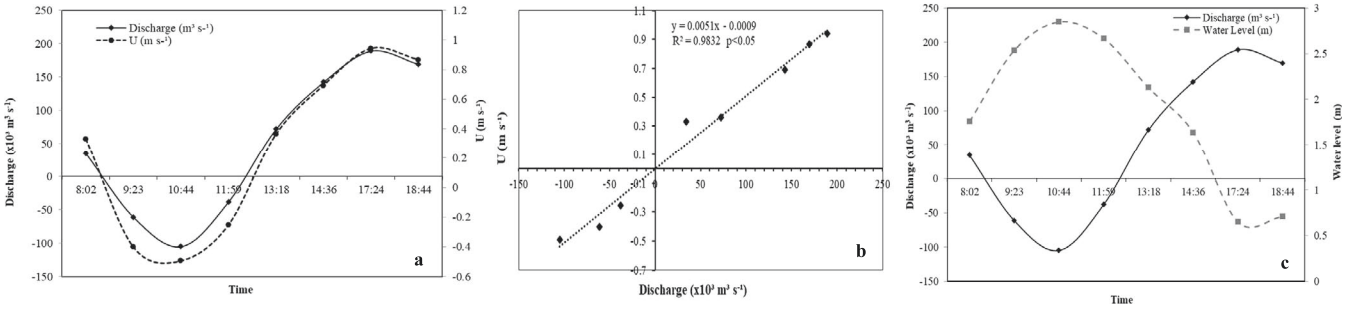

Figure 11. (a) Discharge and water velocity measured during the tidal cycle in the field campaign of October 2015 (low water) in the North Channel of the Amazon River Mouth. (b) Relationship between U and Q ($R^2 = 0.60$, $p < 0.05$). (c) Discharge and water level measured during the tidal cycle.

In general, the highest values of U were observed in the ebb tide in the deepest zones of the channel (Figure 4b,d), which was possibly due to the geomorphology and decreased influence of bed friction (Abreu *et al.*, 2020; Quesada *et al.,* 2019). The variation in discharge and tidal amplitude in the Lower Amazon River can have a strong influence on hydrodynamic characteristics, especially the variation of water velocity, as hypothesized (Quesada *et al.,* 2019; Wang, Sun, and Zhao, 2020). In addition, it is important to note the strong influence of extreme weather events, such as the El Niño periods that occurred between 2015 and 2016 (extreme drought; Cunha and Sternberg, 2018), which increased the influence of the Atlantic Ocean and tides (Santos *et al.,* 2018). The increased tidal influence appeared to spread upstream of the estuary, significantly disrupting the hydrological-hydrodynamic flow pattern and its main physical parameters (Q, U, and h).

The highest discharge values were related to maximum tidal amplitude and water velocities, which reached ~ 3 m and 1.18 m s^{-1}, respectively. The variation in discharge amplifying factors enhanced the tidal amplitude in the Lower Amazon River region and had a strong influence on water velocity dynamics, which, along with the tidal effects, led to a variation in water velocity, as hypothesized. Thus, physical parameters such as river discharge and variation in tidal amplitude in the Amazon estuary appear to be the primary factors determining the hydrological dynamics of the study area (Rosário, Bezerra, and Vinzón, 2009).

CONCLUSIONS

As hypothesized, the results of this study demonstrate the intense influence of seasonal and daily variation of river discharge and tidal amplitude on variability of water velocity in the North Channel near the mouth of the Amazon River. The seasonal and daily influences are also directly related to the seasonality of rainfall when the highest net discharge (124,233 m^3 s^{-1}) was obtained during rising water.

Water velocity reached a maximum of 0.94 m s^{-1} in the hydrological periods with the highest net discharge, when water levels were at their highest. The tidal phase durations demonstrated the intense and predominant influence of river discharge on hydrodynamic characteristics. A significant influence of climatic events that disturbed the hydrodynamic flow pattern in this region (Q, U, and h) was also observed. On the other hand, the hydrodynamic resilience of the flow was verified, even under the impact of a significant hydroclimatic event (El Niño 2015–16, for example). It was possible to observe some similarity between the hydrodynamic flow pattern during hydrologically normal periods and those considered hydrologically under the influence of extreme climatic events.

Considering that hydrodynamics play a relevant role in the physicochemical and biological processes along the Lower Amazon River, this examination of the seasonal and diurnal patterns of tidal river flows provides new insight about the physical characteristics and dynamics of this complex tidal river reach.

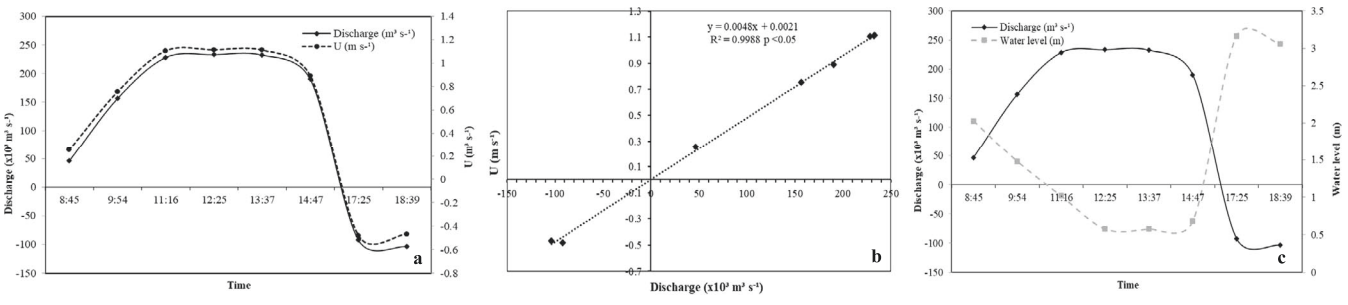

Figure 12. (a) Discharge and water velocity measured during the tidal cycle in the field campaign of May 2016 (high water) in the North Channel of the Amazon River Mouth. (b) Relationship between U and Q ($R^2 = 0.72$, $p < 0.01$). (c) Discharge and water level measured during the tidal cycle.

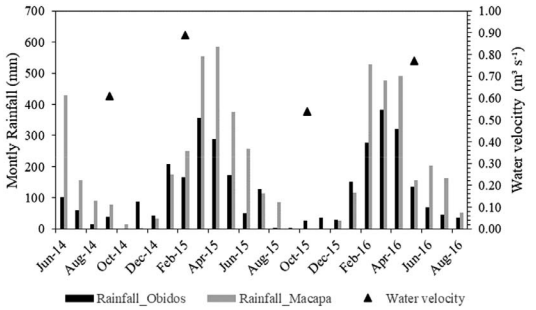

Figure 13. Monthly rainfall in Óbidos and Macapá between 2014 and 2016 and the water velocity measured in the four hydrological periods in the North Channel of the Amazon River Mouth.

Table 3. *Spearman correlations between* Q, U, h, *and depth and correspondent* p *values.*

	Q (m^3 s^{-1})	U (m s^{-1})	h (m)	Depth (m)
Q (m^3 s^{-1})	———	$p < 0.01$	$p < 0.01$	$p < 0.05$
U (m s^{-1})	0.91	———	$p < 0.01$	$p < 0.05$
h (m)	–0.80	–0.72	———	$p > 0.05$*
Depth (m)	–0.40	–0.37	0.13*	———

**No significant correlation occurred between the variables.*

Although this study presents campaign-based hydrodynamic measurements, tropical systems in general lack continuous hydrodynamic monitoring, which will vastly improve the understanding of these critical aquatic systems. Long-term monitoring stations would support the analysis of the influence of hydrodynamics on biogeochemistry, sediment transport, nutrient, and the carbon cycle in this important region in the context of climate change, which campaign-based measurements alone cannot address.

ACKNOWLEDGMENTS

The authors thank Cica and the crew of the B/M Mirage for contributions made during the field campaigns and the project TROCAS- Trocas Líquidas de Carbono do Ecossistema do Baixo Rio Amazonas. The authors are also grateful to the Laboratory of Chemistry, Sanitation and Environmental Systems Modeling (LQSMSA) and thank DPq/PROPESPg/UNIFAP and FUNASA (TR-2018).

This research was funded by National Council for Scientific and Technological Development (CNPq) Grant Number: 309684/2018-8; Amapá Research Foundation (FAPEAP); FAPESP grant: 08/58089-9; and NSF DEB, Grant: 791 #1256724.

LITERATURE CITED

Abreu, C.H.M.; Brito, D.C.; Barros, M.L.C.; Teixeira, M.R., and Cunha, A.C., 2020. Hydrodynamic modeling and simulation of water residence time in the Estuary of the Lower Amazon River. *Water,* 12(3), 1–30. doi:10.3390/w12030660

Abril, G.; Deborde, J.; Savoye, N.; Mathieu, F.; Moreira-Turcq, P.; Artigas, F.; Meziane T.; Takiyama, L.R.; Souza, M.S., and Seyler, P., 2013. Export of 13C-depleted dissolved inorganic carbon from a tidal forest bordering the Amazon estuary. *Estuaries, Coastal and Shelf Sciences,* 129, 23–27. doi:10.1016/j.ecss.2013.06.020

Abril, G.; Etcheber, H.; Borges, A.V., and Frankignoulle, M., 2000. Excess atmospheric carbon dioxide transported by rivers into the Scheldt Estuary. *Comptes Rendus Géosciences,* 330(11), 761–768. doi:10.1016/S1251-8050(00)00231-7

Alfredini, P. and Arasaki, E., 2009. *Obras e gestão de portos e costas*: A técnica aliada ao enfoque logístico e ambiental. São Paulo: Blucher, 804p.

Borges, A.V., 2005. Do we have enough pieces of the jigsaw to integrate CO_2 fluxes in the coastal ocean? *Estuaries* 28(1), 3–27. doi:10.1007/BF02732750

Borges, A.V. and Abril, G., 2011. *Treatise on Coastal and Estuarine Science*. London, UK: Academic, 4590p.

Braunschweig, F.; Martins, F.; Neves, R.; Pina, P.; Santos, M., and Saraiva, S.A., 2003. *Importância dos Processos Físicos no controlo da Eutrofização em Estuários*. Liboa, PT: INAG-Instituto da Água, 4p.

Cai, W., 2011. Estuarine and coastal ocean carbon paradox: CO_2 sinks or sites of terrestrial carbon incineration? *Annual Review of Marine Science,* 3(1), 123–145. doi:10.1146/annurev-marine-120709-142723

Cai, W-J.; Pomeroy, L.R.; Moran, M.A., and Wang, Y.C., 1999. Oxygen and carbon dioxide mass balance for the estuarine-intertidal marsh complex of five rivers in the southeastern U.S. *Limnology and Oceanography,* 44(3), 639–649. doi:10.4319/lo.1999.44.3.0639

Callède, J.; Guyot, J.L.; Ronchail, J.; Molinier, M., and Oliveira, E., 2002. L'Amazone à Óbidos (Brésil): Étude statistique des débits et bilan hydrologique. *Hydrological Sciences Journal,* 47(2), 321–333. doi:10.1080/02626660209492933

Chen, C.T.A.; Huang, T.H.; Chen, Y.C.; Bai, Y.; He, X., and Kang, Y., 2013. Air–sea exchanges of CO_2 in the world's coastal seas. *Biogeosciences,* 10(10), 6509–6544. doi:10.5194/bg-10-6509-2013

Chong, L.S.; Berelson, W.M.; Hammond, D.E.; Fleisher, M.Q.; Anderson, R.F.; Rollins, N.E., and Lund, S., 2016. Biogenic sedimentation and geochemical properties of deep-sea sediments of the Demerara Slope/Abyssal Plain: Influence of the Amazon River Plume. *Marine Geology,* 379, 124–139. doi:10.1016/j.margeo.2016.05.015

Costa, A.C.L.; Silva Junior, A.A.; Cunha, A.C.; Galbrarth, D.; Feitosa, J.R.P., and Mattos, A., 2013. Distribuição geoespacial e horária da temperatura do ar na cidade de Belém-PA. *Brazilian Geographical Journal,* 4(1), 150–168.

Cotovicz, L.C.; Libardonia, B.G.; Brandinia, N.; Knoppersa, B.A., and Abril, G., 2016. Comparações entre medições em tempo real da pCO_2 aquática com estimativas indiretas em dois estuários tropicais contrastantes: o estuário eutrofizado da Baía de Guanabara (RJ) e o estuário oligotrófico do Rio São Francisco (AL). *Química Nova,* 39(10), 1206–1214. doi:10.21577/0100-4042.20160145

Cunha, A.C.; Brito, D.C.; Brasil Junior, A.C.; Pinheiro, L.A.R.; Cunha, H.F.A., and Krusche, A.V., 2012. Challenges and solutions for hydrodynamic and water quality in rivers in the Amazon Basin. *In:* Schulz, H.E.; Simões, A.L.A., and Rijeka, J. (eds.), *Hydrodynamics: Natural Water Bodies*. Croatia: InTech, 302p.

Cunha, A.C.; De Abreu, C.H.M.; Crizanto, J.L.P.; Cunha, H.F.A.; Brito, A.U., and Pereira, N.N., 2021. Modeling pollutant dispersion scenarios in high vessel-traffic areas of the Lower Amazon River. *Marine Pollution Bulletin,* 168, 112404. doi:10.1016/j.marpolbul.2021.112404

Cunha, A.C. and Sternberg, L.S.L., 2018. Using stable isotopes O^{18} and H^2 and biogeochemical analysis to identify factors affecting water quality in four estuarine Amazonian shallow lakes. *Hydrological Process,* 32(9), 1188–1201. doi:10.1002/hyp.11462

Eom, J.; Seo, K.W., and Ryu, D., 2017. Estimation of amazon river discharge based on EOF analysis of grace gravity data. *Remote Sensing Environment,* 191, 55–66. doi:10.1016/j.rse.2017.01.011

Fisch, G.; Marengo, J.A., and Nobre, C.A., 1998. Uma Revisão Geral Sobre o Clima da Amazônia. *Acta Amazonica,* 28(2),101–126. doi:10.1590/1809-43921998282126

Frankignoulle, M.; Abril, G.; Borges, A.; Bourge, I.; Canon, C.; Delille, B.; Libert, E., and Théate, J., 1998. Carbon dioxide emission from European estuaries. *Science,* 282(5388), 434–436. doi:10.1126/science.282.5388.434

Freitas, P.T.A.; Asp, N.E.; Souza-Filho, P.W.M.; Nittrouer, C.A.; Ogston, A.S., and Silva, M.S., 2017. Tidal influence on the hydrodynamics and sediment entrapment in a major Amazon River tributary—Lower Tapajós River. *Journal of South American Earth Sciences,* 79, 189–201. doi:10.1016/j.jsames.2017.08.005

Gabioux, M.; Vinzon, S.B., and Paiva, A.M., 2005. Tidal propagation over fluid mud layers on the Amazon shelf. *Continental Shelf Research,* 25(1), 113–125. doi:10.1016/j.csr.2004.09.001

Gagne-Maynard, W.; Ward, N.D.; Keil, R.G.; Sawakuchi, H.O.; Cunha, A.C.; Neu, V.; Brito, D.C.; Less, D.F.S.; Diniz, J.E.; Matos, A.; Kampel, M.; Krusche, A.V., and Richey, J.E., 2017. Evaluation of primary production in the Lower Amazon River based on a sissolved oxygen stable isotopic mass balance. *Frontiers in Marine Science,* 4, 1–12. doi:10.3389/fmars.2017.00026

Garel, E. and D'alimonte, D., 2017. Continuous river discharge monitoring with bottom-mounted current profilers at narrow tidal estuaries. *Continental Shelf Research,* 133, 1–12. doi:10.1016/j.csr.2016.12.001

Gloor, M.; Brienen, R.J.W.; Galbraith, D.; Feldpausch, T.R.; Schongart, J.; Guyot, J-L.; Espinoza, J.C.; Lloyd, J., and Phillips, O.L., 2013. Intensification of the Amazon hydrological cycle over the last two decades. *Geophysic Research Letters,* 40(9), 1729–1733. doi:10.1002/grl.50377

Guyot, J.L.; Filizola, N., and Guimarães, V., 1998. Amazon suspended sediment yield measurements using an Acoustic Doppler Current Profiler (ADCP): First results. *In:* Johnson, A.I. and Fernandez-Jauregui, C.A. (eds.) *Hydrology in the Humid Tropic Environment*. Kingston, Jamaica: IAHS.

Haslet, S.K., 2009. *Coastal Systems*. New York: Routledge, 240p.

Ji, H.; Pan, S., and Chen, S., 2020. Impact of river discharge on hydrodynamics and sedimentary processes at Yellow River Delta. *Marine Geology,* 425(106210), 1–14. doi:10.1016/j.margeo.2020.106210

Jiménez-Muñoz, J.; Mattar, C.; Barichivich, J.; Artigas, A.S.; Takahashi, K.; Yadvinder, M.; Sobrino, J.A., and Van Der Schrier, G., 2016. Record-breaking warming and extreme drought in the Amazon rainforest during the course of El Niño 2015–2016. *Scientific Reports,* 6(33130), 1–7. doi:10.1038/srep33130

Köppen, W., 2020. Das geographische system der klimate. *In:* Köppen W. and Geiger R. (eds.), *Handbuch der Klimatologie*. Berlin, Germany: Gerbrüder Borntraeger, 1936(1), 44.

Kosuth, P.; Callède, J.; Laraque, A.; Filizola, N.; Guyot, J-L.; Seyler, P.; Fritsch, J-M., and Guimarães, V., 2009. Sea-tide effects on flows in the lower reaches of the Amazon River. *Hydrological Process,* 23(22), 3141–3150. doi:10.1002/hyp.7387

Liebmann, B. and Marengo, J., 2001. Interannual variability of the rainy season and rainfall in the Brazilian Amazon Basin. *Journal Climate,* 14(22), 4308–4318. doi:10.1175/15200442(2001)014<4308:IVOTRS>2.0.CO;2

Marengo, J.A., 2009. Long-term trends and cycles in the hydrometeorology of the Amazon basin since the late 1920s. *Hydrological Process,* 23(22), 3236–3244. doi:10.1002/hyp.7396

Marengo, J.A. and Espinoza, J.C., 2015. Extreme seasonal droughts and floods in Amazonia: Causes, trends and impacts. *International Journal of Climatology,* 36(3), 1033–1050. doi:10.1002/joc.4420

Marengo, J.A.; Tomasella, J.; Soares, W.R.; Alves, L.M., and Nobre, C., 2011. Extreme climatic events in the Amazon basin. *Theoretical and Applied Climatology,* 107(1–2), 73–85. doi:10.1007/s00704-011-0465-1

Matte, P.; Secretan, Y., and Morin, J., 2014. Temporal and spatial variability of tidal-fluvial dynamics in the St. Lawrence fluvial estuary: An application of nonstationary tidal harmonic analysis. *Journal of Geophysical Research-Oceans,* 119(9), 5724–5744. doi.org/10.1002/2014JC009791

Molinas, E.; Vinzon, S.B.; Vilela, C.D.X., and Gallo, M.N., 2014. Structure and position of the bottom salinity front in the Amazon Estuary. *Ocean Dynamics,* 64, 1583–1599. doi:10.1007/s10236-014-0763-0

Montagna, P.; Palmer, T.A., and Pollack, J., 2013. *Hydrological Changes and Estuarine Dynamics*. New York: Springer-Verlag, 105p.

McLusky, D.S. and Elliott, M., 2004. *The Estuarine Ecosystem: Ecology, Threats and Management*. New York: Oxford University Press, 222p.

National Institute of Meteorology—INMET, 2021. *Meteorological Database*. http://www.inmet.gov.br/portal/index.php?r=bdmep/bdmep

National Institute of Meteorology—INMET, 2020. *Historical Average of Precipitation (1981 to 2010)*. https://portal.inmet.gov.br/normais

Quesada, M.C.C.; García-Lafuente, J.; Garel, E.; Cabello, J.D.; Martins, F., and Moreno-Navas, J., 2019. Effects of tidal and river discharge forcings on tidal propagation along the Guadiana Estuary. *Journal of Sea Research,* 146, 1–13. doi:10.1016/j.seares.2019.01.006

R Project for Statistical Computing, 2021. *The R Project for Statistical Computing*. http://www.r-project.org

Raymond, P.A.; Hartmann, J.; Lauerwald, R.; Sobek, S.; McDonald, C.; Hoover, M.; Butman, D.; Striegl, R.; Mayorga, E.; Humborg, C.; Kortelainen, P.; Dürr, H.; Meybeck, M.; Ciais, P., and Guth, P., 2013. Global carbon dioxide emissions from inland waters. *Nature,* 503, 355–359. doi:10.1038/nature12760

Richey, J.E.; Melack, J.M.; Aufdenkampe, A.K.; Ballester, V.M., and Hess, L.L., 2002. Outgassing from Amazonian rivers and wetlands as a large tropical source of atmospheric CO_2. *Nature,* 416(6881), 617–620. doi:10.1038/416617a

Richey, J.E.; Spencer, R.; Drake, T.W., and Ward, N.D., 2021. Fluvial carbon dynamics across the land to ocean continuum of great tropical rivers: the Amazon and Congo. AGU Monograph Series. *In:* Alsdorf, D.E.; Tshimanga, R., and Moukandi, G. (eds.), *Congo Basin Hydrology, Climate, and Biogeochemistry: A Foundation for the Future*. Malden, Massachusetts: AGU Books, pp. 1–53. doi:10.1002/essoar.10505912.1

Rosário, R.P.; Bezerra, M.O., and Vinzón, S.B., 2009. Dynamics of the saline front in the northern channel of the Amazon River—Influence of fluvial flow and tidal range (Brazil). *In:* da Silva, C.P. (ed.), *Proceedings from the International Coastal Symposium (ICS) 2009,* Special Issue No. 56, 1414–1418. http://www.jstor.org/stable/25738022

Santos, E.S.; Pinheiro, P.P.L.; Pereira, H.H.S.; Nascimento, O.O.; Rennie, C.D.; Sternberg, L.S.L.O., and Cunha, A.C., 2018. The impact of channel capture on estuarine hydro-morphodynamics and water quality in the Amazon delta. *Science of Total Environment,* 624, 887–899. doi:10.1016/j.scitotenv.2017.12.211

Sassi, M.G. and Hoitink, A.J.F., 2013. River flow controls on tides and tide-mean water level profiles in a tidal freshwater river. *Journal of Geophysical Research: Oceans,* 118(9), 4139–4151. doi:10.1002/jgrc.20297

Sawakuchi, H.O.; Neu, V.; Ward, N.D.; Barros, M.L.C.; Valerio, A.M.; Gagne-Maynard, W.; Cunha, A.C.; Less, D.F.S.; Diniz, J.E.M.; Brito, D.C.; Krusche, A.V., and Richey, J.E., 2017. Carbon dioxide emissions along the lower Amazon River. *Frontiers in Marine Science,* 4, 1–12. doi:10.3389/fmars.2017.00076

Schöngart, J. and Junk, W.J., 2007. Forecasting the flood-pulse in Central Amazonia by ENSO-Índices. *Journal of Hidrology,* 335(1), 124–132. doi:10.1016/j.jhydrol.2006.11.005

Vale, R.S.; Gomes, A.C.; Santana, R.A.S.; Tóta, J.; Miller, S.D., and Sousa, R.A.F., 2016. Hydroclimatic variables associated with El Nino and La Nina events at the Curuá-Una hydroelectric reservoir, Central Amazonia. *Acta Amazonica,* 46(3), 303–308. doi:10.1590/1809-4392201600083

Valerio, A.M.; Kampel, M.; Vantrepotte, V.; Ward, N.D.; Sawakuchi, H.O.; Less, D.F.S.; Neu, V.; Cunha, A.C., and Richey, J.E., 2018. Using CDOM optical properties for estimating DOC concentrations and pCO_2 in the Lower Amazon River. *Optics Express,* 26(14), A657–A677. doi:10.1364/OE.26.00A657

Valerio, A.M.; Kampel, M.; Ward, N.D.; Sawakuchi, H.O.; Cunha, A.C., and Richey, J.E., 2021. CO2 partial pressure and fluxes in the Amazon River plume using in situ and remote sensing data. *Continental Shelf Research*, 215, 104348. doi:10.1016/j.csr.2021.104348

Wang, H. and Fu, R., 2007. The influence of Amazon rainfall on the Atlantic ITCZ through convectively coupled Kelvin waves. *Journal of Climate,* 20(7), 1188–1201. doi:10.1175/JCLI4061.1

Wang, X.; Sun, J., and Zhao, Z., 2020. Effects of river discharge and tidal meandering on morphological changes in a meso tidal creek. *Estuarine, Coastal and Shelf Science,* 234(106635), 1–10. doi:10.1016/j.ecss.2020.106635

Ward, N.D.; Bianchi, T.S.; Medeiros, P.M.; Seidel, M.; Richey, J.E.; Keil, R.G., and Sawakuchi, H.O., 2017. Where carbon goes when water flows: Carbon cycling across the aquatic continuum. *Frontiers in Marine Science*. 4(7). doi:10.3389/fmars.2017.00007

Ward, N.D.; Bianchi, T.S.; Sawakuchi, H.O.; Gagne-Maynard, W.; Cunha, A.C.; Brito, D.C.; Neu, V.; De Matos, A.V.; Da Silva, R.; Krusche, A.V.; Richey, J.E., and Keil, R.G., 2016. The reactivity of plant-derived organic matter and the potential importance of priming effects along the lower Amazon River. *Journal of Geophysical Research: Biogeosciences,* 121(6), 1522–1539. doi:10.1002/2016JG003342

Ward, N.D.; Krusche, A.V.; Sawakuchi, H.O.; Brito, D.C.; Cunha, A.C.; Moura, J.M.S.; Da Silva, R.; Yager, P.L.; Keil, R.G., and Richey, J.E., 2015. The compositional evolution of dissolved and particulate organic matter along the lower Amazon River—Óbidos to the ocean. *Marine Chemistry,* 177(Part 2), 244–256. doi:10.1016/j.marchem.2015.06.013

Ward, N.D.; Megonigal, J.P.; Bond-Lamberty, B.; Bailey, V.; Butman, D.; Canuel, E.A.; Diefenderfer, H.; Ganju, N.K.; Goñi, M.A.; Graham, E.B.; Hopkinson, C.S.; Khangaonkar, T.; Langley, J.A.; McDowell, N.G.; Myers-Pigg, A.N.; Neumann, R.B.; Osburn, C.L.; Price, R.M.; Rowland, J.; Sengupta, A.; Simard, M.; Thornton, P.E.; Tzortziou, M.; Vargas, R.; Weisenhorn, P.B., and Windham-Myers, L., 2020. Representing the function and sensitivity of coastal interfaces in Earth system Models. *Nature Communications*, 11(2458). doi:10.1038/s41467-020-16236-2

Ward, N.D.; Sawakuchi, H.O.; Neu, V.; Less, D.F.S.; Valerio, A.M.; Cunha, A.C.; Kampel, M.; Bianchi, T.S.; Krusche, A.V.; Richey, J.E., and Keil, R.G., 2018. Velocity-amplified microbial respiration rates in the lower Amazon River. *Limnology and Oceanography,* 3(3), 265–274. doi:10.1002/lol2.10062

Wollast, R., 1998. Evaluation and comparison of the global carbon cycle in the coastal zone and in the open ocean. *In:* Brink, K.H. and Robinson, A.R. (ed.), *The Sea: the Global Coastal Ocean*. New York: Wiley, 1090p.

Zhang, F.; Sun, J.; Lin, B., and Huang, G., 2018. Seasonal hydrodynamic interactions between tidal waves and river flows in the Yangtze Estuary. *Journal of Marine Systems,* 186, 17–28. doi:10.1016/j.jmarsys.2018.05.005